PAPER

Check for updates

High-pressure ilmenite-type MnVO₃: crystal and spin structures in the itinerant-localized regimes†

Elena Solana-Madruga, [ID] [ab] Olivier Mentré, [ID] [a] Eugenia P. Arévalo-López, [c] Dmitry Khalyavin, [ID] [d] Francois Fauth, [ID] [e] Alexandr Missiul [e] and Angel M. Arévalo-López [ID] *[a]

Herein we report the Peierls-like transition in the high-pressure ilmenite-type MnVO₃. The first-order structural transition from a low-temperature $P\bar{1}$ to a high-temperature $R\bar{3}$ occurs at 475 K, accompanied by a semiconductor to metal-like transition. The triclinic distorted phase presents a V–V dimerization with a short ~2.85 Å bond formation at 300 K. Below 80 K MnVO₃ orders antiferromagnetically with a small ferromagnetic component. Neutron diffraction reveals that both Mn and V cations contribute to the magnetic ordering, contrary to what expected on the V–V dimer formed. Extended Hückel and DFT calculations expose that the formation of covalent pairing is only partially achieved, contrary to the MgVO₃ and CoVO₃ counterparts.

Introduction

Transition metal oxides with ABO₃ stoichiometry are intensively studied due to their chemical, structural and functional versatility. A wide variety of crystal structures accepting different degrees of distortion can be stabilized, mainly depending on the relative ionic radii of A- and B-site cations, as defined by the Goldschmidt relation.[1] Synthesis conditions can also induce notable effects on the preferred crystallization of the compounds with different structures. In particular, high-pressure and high-temperature synthesis provides accessibility to metastable compounds with unusual oxidation states and metal coordinations. Small cations can also be stabilised into large voids.[2,3] This is the case, for instance, of A-site manganites, where perovskite and corundum related structures are reported with a rich variety of cation ordered superstructures.[4]

Two high pressure polymorphs of MnVO₃ were first reported in 1970. The initial structural characterization revealed a triclinic

distortion $P\bar{1}$ of an ilmenite-type structure (MnVO₃-I) and an orthorhombic (*Pnma*) perovskite (MnVO₃-II) for the low- and the high-pressure phases below and above 4 GPa respectively.[5] It was not until 2011 when MnVO₃-II, the only quenchable simple perovskite with Mn²⁺ in the A site, was fully understood. It showed a complex behaviour with spin polarized conduction electrons and an incommensurate magnetic structure in a half-metallic state.[6]

MnVO₃-I however, has not been fully understood. It belongs to the AVO₃ with A = Mg, Mn, Co, Ni and Cu high-pressure triclinic ilmenites.[7–9] MgVO₃ and CoVO₃ exhibit a ladder-like V–V dimerization and non-magnetic singlet ground states with a concomitant triclinic to rhombohedral phase transformations at 500 and 550 K respectively.[10,11] NiVO₃ and CuVO₃ have not been fully studied.[9,12,13]

MnVO₃-I has been recently obtained in single-crystal form from a solid-state recrystallization under high-pressure and high-temperature conditions.[14] The ladder-like V–V dimerization pattern is also observed in this phase. Here we present a complete characterization of bulk MnVO₃-I, including the thermal evolution of its physical properties and ground-state magnetic structure. A comparative study against the related MgVO₃ and CoVO₃ is performed to discuss the observed behaviour. Unprecedented magnetic order into the V sublattice is observed despite the presence of V–V dimers, which is justified in terms of a combination of correlation-(Mott) and band-effects (Peierls) in the low temperature triclinic semiconducting phase against the metallic-like high temperature rhombohedral polymorph, similar to the VO₂ scenario.[15–19]

[a] *UMR-8181-UCCS-Unité de Catalyse et Chimie du Solide-Univ. Lille, CNRS, Centrale Lille, ENSCL, Univ. Artois, Lille F-59000, France. E-mail: angel.arevalo-lopez@univ-lille.fr*

[b] *Dpto. Q. Inorgánica, Facultad CC. Químicas, Universidad Complutense de Madrid, Avda. Complutense sn, 28040, Madrid, Spain*

[c] *Facultad de Ciencias, Universidad Nacional Autónoma de Mexico, A.P. 70-399, Cd, Mexico 04510, Mexico*

[d] *ISIS Facility, Rutherford Appleton, Laboratory, Harwell, Didcot, Oxford OX11 0QX, UK*

[e] *CELLS-ALBA synchrotron, Carrer de la Llum 2-26, 08290Cerdanyola del Vallés, Barcelona, Spain*

† Electronic supplementary information (ESI) available: Tables and figures for the low and high temperature polymorphs are included. CCDC 2259432. For ESI and crystallographic data in CIF or other electronic format see DOI: https://doi.org/10.1039/d3tc01541f

Experimental

Pollycrystalline MnVO₃-I was obtained at 4 GPa and 1273 K for 30 minutes using a Walker-type multianvil press, further details

9238 | *J. Mater. Chem. C*, 2023, **11**, 9238–9244

This journal is © The Royal Society of Chemistry 2023

concerning this technique are given in the ESI.† Stoichiometric amounts of MnO (99.9% Sigma-Aldrich) and VO_2 were placed in a Pt capsule and into the press. VO_2 was prepared from a 1:1 V_2O_3:V_2O_5 mixture in vacuum at 700 °C for 24 h, and V_2O_3 was previously obtained *via* reduction of V_2O_5 (99.9% Sigma-Aldrich) under hydrogen at 700 °C. Synchrotron X-ray radiation powder diffraction (SXRPD) was performed at the BL04 MSPD beamline of ALBA synchrotron in Spain. Data were collected using a $\lambda = 0.4142$ Å wavelength in the $0° < 2\theta < 40°$ angular range with a 0.006° effective step size.[20,21] High-resolution neutron powder diffraction (NPD) data were collected in a combination of several high-pressure experiment runs (63 mg in total) in the WISH diffractometer at the ISIS facility.[22] Long scans were obtained at 2 K and 100 K and shorter scans were collected every 3 K on warming. Rietveld refinements were performed using Fullprof Suite.[23]

Single-crystal data from isolated small crystals was collected on a Bruker DUO diffractometer (Mo K_α radiation) and treated using the JANA 2006 software.[24]

X-ray photoelectron spectroscopy (XPS) analyses were carried out in an ultra-high vacuum (UHV) system Scanning XPS microprobe PHI 5000 VersaProbe II, with an Al K_α X-ray source ($h\nu = 1486.6$ eV) monochromatic with 200 μm beam diameter, and a Multi-Channel Detector (MCD) analyzer. EDX analysis were also performed in a FLEXSEM 1000, see ESI† for further details.

Magnetic properties were measured using a PPMS 9T Dynacool from Quantum Design. Magnetization was measured in ZFC-FC mode under 0.1 T and hysteresis loops collected at several temperatures. Heat capacity was measured on an as-obtained pellet between 2 and 300 K and corrected with an addendum. Resistivity measurements were performed using a 4-probe system with a Keithley 6221 source and a 2182A Nanovoltmeter installed in a Linkam high temperature station.

Extended Hückel tight-binding calculations (EHTB) have been performed using the SAMOA package.[25] DFT+U calculations were performed with the general gradient approximation (GGA) using the popular Perdew–Burke–Ernzerhof (PBE) approach in the Vienna *ab initio* simulation package (VASP).[26] Extra on-site electron–electron Coulomb interactions were also considered with the GGA+U approach implemented in the code. Crystal structures were optimized by minimizing the total energy, phonon dispersions calculations were not performed to test dynamical stability of the optimized structures. The lattices and atomic positions were relaxed starting from the 300 K and the 560 K MnVO₃-I refined models, within a convergence force criterion of 3×10^{-2} eV Å^{-1}. The relaxed lattice contraction $\Delta V/V_0$ are 6.5% and 4.9% for the rhombohedral and triclinic cells respectively, as commonly found for DFT. It was checked that the experimental low temperature triclinic phase is most stable by ~ 40 meV per formula unit, compared to the rhombohedral form. For electronic calculations, we assume the most stable AFM state with $U = 1$ eV for Mn and V atoms. The electrons Mn, V (3s, 3p, 3d, 4s) and O (2s, 2p) were treated as valence states. The cutoff energy for the plane-wave-basis is 400 eV, and the total energy of the system was converged with respect to the plane-wave cutoff energy and reciprocal space samplings. The free-energy convergence criterion was set to 10^{-10} eV using a Γ-centered $8 \times 8 \times 8$ Monkhorst-Pack k-point mesh. A systematic revision of all possible spin configurations was not pursued, but can be performed in future theoretical studies aiming a further understanding of the transition mechanism.

Results and discussion

$MnVO_3$-I was synthesized under high-pressure and high-temperature conditions as described in the experimental section
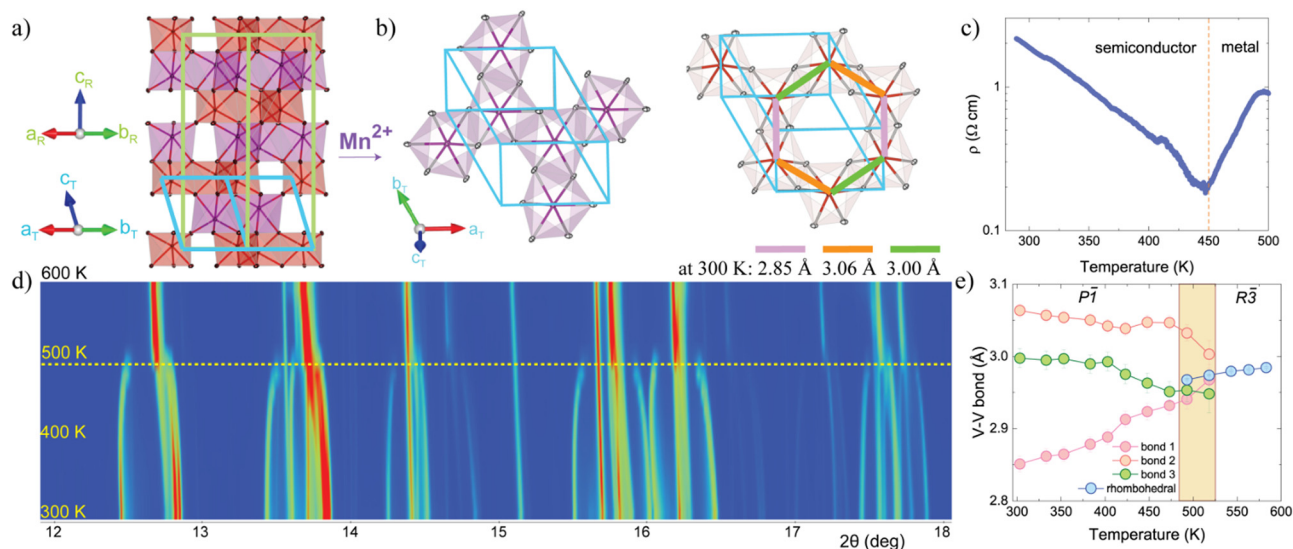
Fig. 1 (a) Crystal structure of MnVO₃-I viewed along the [110] in the rhombohedral high-temperature cell (green axes). (b) Cobalt and vanadium honeycomb-layers viewed along the c_T^* direction of the triclinic (blue) cell, identifying the three different V–V bonds with a ladder pattern and their lengths at 300 K. (c) Resistivity of a MnVO₃-I pellet fragment at high temperature in a semi-log representation. It shows a transition from semiconducting to a metallic state on heating at 450 K. (d) Thermal evolution of the SXRD patterns on warming between 300 and 600 K. (e) Temperature dependence of V–V lengths obtained from the refined crystal structure with a coexistence of both phases in the shaded area.

This journal is © The Royal Society of Chemistry 2023

J. Mater. Chem. C, 2023, **11**, 9238–9244 | **9239**

above. Small single crystals were successfully isolated for structural determination at room temperature (CCDC 2259432†) in good agreement with the recently reported MnVO$_3$ crystal structure.[14] The model obtained by single crystal (Table S1, ESI†) was subsequently used in the Rietveld refinements of SXRPD and NPD data and results are summarized in ESI.† MnVO$_3$-I crystallizes in the $P\bar{1}$ space group with $a = 5.0177(7)$ Å, $b = 5.0513(7)$ Å, $c = 5.5210(8)$ Å, $\alpha = 116.679(6)°$, $\beta = 90.044(6)°$ and $\gamma = 118.924(5)°$ cell parameters at 300 K. The structure is shown in Fig. 1a and b. It presents a distorted ilmenite-type structure, as the MgVO$_3$ and CoVO$_3$.[10,11] The low symmetry in MnVO$_3$-I arises from the distortion of the Mn and V honeycomb lattices. Three different V–V lengths are observed, two long (3.025(1) Å and 3.00(1) Å) and one short (2.849(1) Å) at 300 K. The short length of the V–V pair is still comparable to those of the related MgVO$_3$ (~ 2.78 Å) and CoVO$_3$ (~ 2.74 Å). This agrees with the ionic radius of the different A cations, 0.72, 0.745 and 0.83 Å for Mg, Co and Mn respectively. Moreover, the short V–V bond is below the critical interatomic distance ($R_c \sim 2.94$ Å) for which direct metal–metal bond may be formed in vanadium oxides,[27,28] thus structural clues for V–V dimerization exist in MnVO$_3$-I. The Mn sublattice shows no formation of dimerized features exhibiting a narrow distribution of Mn–Mn distances (3.065(1), 3.017(1) and 2.964(1) Å at 300 K). The calculated bond valence sum (BVS)[29] results in $\sim 2.08+$ for Mn and $\sim 3.47+$ for V. This reflects the stressed structure obtained in a high-pressure metastable phase. EDX and XPS measurements respectively support the expected composition and formal oxidation states Mn^{2+}V^{4+}O$_3^{2-}$, see ESI.†

Fig. 1d shows a small angular range for the thermal evolution of the SXRPD patterns between 300 and 600 K. A reversible first order structural phase transition from triclinic ($P\bar{1}$) to rhombohedral ($R\bar{3}$) ilmenite-type structure occurs at 475 K with a coexistence of both phases up to 525 K. Refined atomic positions confirm the presence of V–V dimers as revealed by interatomic distances in Fig. 1e. In the rhombohedral phase the dimerization is vanished by symmetry, resulting in a V–V and Mn–Mn distances of 2.984(9) Å and 2.960(6) Å respectively at 560 K. The transformation matrix between the triclinic $P\bar{1}$ and rhombohedral $R\bar{3}$ polymorphs used in here is: $(a', b', c')_R = (a,b,c)_T [1\ 0\ 1,\ 0\ 1\ 2,\ 0\ 0\ 3]$.

The cell parameters and the volume (ESI†) exhibit a change at the transition and both structures coexist in the 475–525 K temperature range proving that it is of first order. Fig. 1c shows the electrical resistivity measurements at high temperatures with a clear change from a semiconductor to a metal-like transition at 450 K on heating. However, one should be careful, since this could just mean that the carrier mobility is strongly affected by scattering with phonons and/or defects as temperature increases. It is however 25 K below the structural transition, suggesting that the electronic correlations (Mott) may need to be lost before the structural change can occur (Peierls). This somehow resembles the dynamical dimer state in MgVO$_3$, where a difference of ~ 100 K between the magnetic and the structural transition was reported.[10] Moreover, MgVO$_3$ shows a change from a Pauli-paramagnetic (metal) to a non-magnetic dimerized state (semiconductor). Thus, by analogy, suggesting

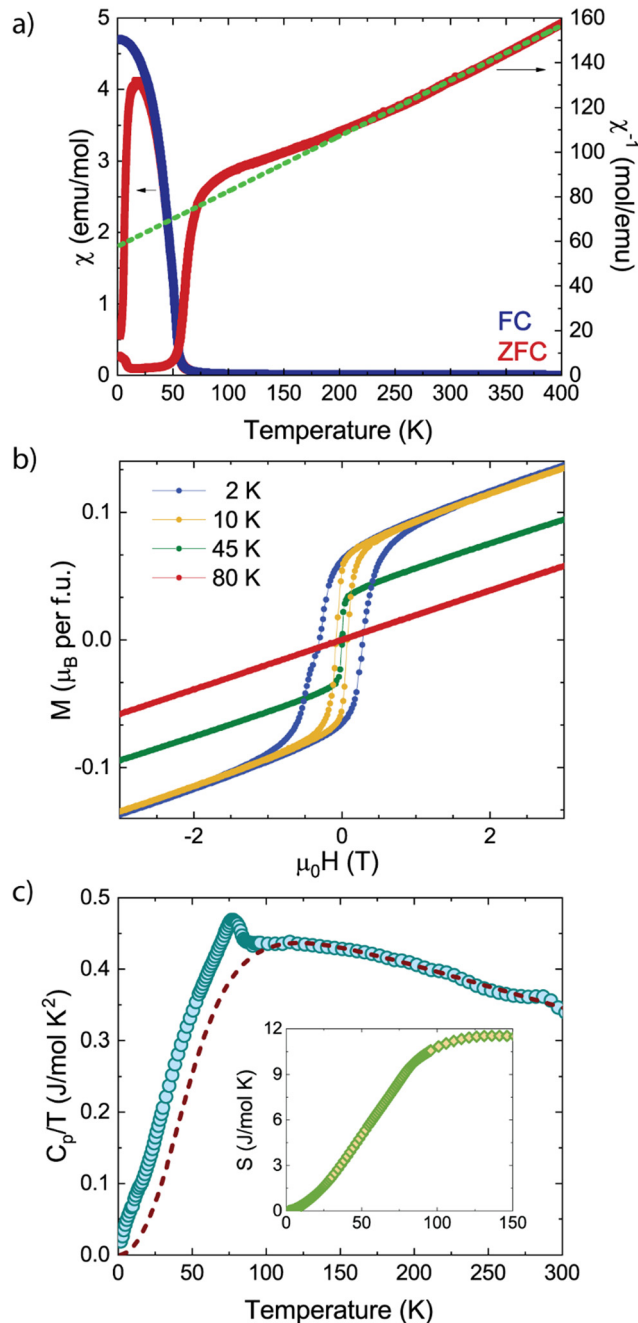Fig. 2 (a) Temperature dependence of the zero-field (ZFC, red) and field cooling (FC, blue) magnetic susceptibilities of MnVO$_3$-I in a 0.1 T external applied field. The inverse susceptibility shows the results of a Curie-Weiss fit. (b) Field dependent magnetization at different temperatures. (c) Specific heat divided by temperature (blue dots) along with the lattice contributions (dashed purple line). Inset shows the calculated entropy.

the observed electronic transition at 450 K in MnVO$_3$-I involves metallization. It is also similar to the metal–insulator transition in VO$_2$, where the dimerization and the electron correlations break at the transition.[16]

Low temperature dependent magnetization measurements for MnVO$_3$-I in 0.01 T external field (Fig. 2a) show a ferrimagnetic transition at $T_N = 77(1)$ K. The Curie–Weiss fit of the

9240 | J. Mater. Chem. C, 2023, 11, 9238–9244

This journal is © The Royal Society of Chemistry 2023

inverse susceptibility above 250 K shows a paramagnetic moment of 5.7(1) μ_B f.u.$^{-1}$, close to the theoretical value of 5.92 μ_B when considering only Mn^{2+}. Weiss temperature of θ_W = −233(1) K demonstrates that antiferromagnetic spin–spin interactions are dominant but partially frustrated ($|\theta|/T_N \approx 3$). Magnetic hysteresis loops below T_N developed a weak ferromagnetic (WFM) component with a remnant magnetization of $0.07\mu_B$ at 2 K. Heat capacity measurements present a lambda-like peak at 77 K in agreement with the WFM transition, see Fig. 2c. Assuming the vanadium atoms are in a dimerized singlet state and after the phonon contribution was subtracted, the magnetic entropy released of 11(1) J mol^{-1} K^{-1} accounts for 3/4 of the theoretical value $S = R\ln(2S + 1) = 14.9$ J mol^{-1} K^{-1} for MnVO$_3$-I.

Mn$_3$V$_2$O$_8$ minority phase presents a transition at 21 K,[30] which appears below the ferrimagnetic transition of MnVO$_3$-I (T_N = 77 K). Thus, the observed features in our experimental data are intrinsic to our sample. Refinements of neutron diffraction data consider the impurity phase, thus ensuring its presence does not affect the interpretation of the magnetic properties.

The temperature dependence of the MnVO$_3$-I NPD data reveals the appearance of magnetic peaks below T_N = 77 K, see ESI.† These extra reflections coincide with the crystal structure and can be indexed with propagation vector k_0 = [0 0 0] (Γ point of the first Brillouin zone). ISODISTORT was used to determine the possible magnetic structures and space group.[31,32] The final Rietveld fit was obtained with Fullprof with the mΓ1$^-$ irreducible representation with the triclinic $P\bar{1}'$ magnetic space group (2.6).

The magnetic structure, depicted in Fig. 3, can be described as AFM layers of Mn and V atoms. The refined ordered magnetic moments (R_{mag} = 2.71%, χ^2 = 1.49) at 2 K converge to 3.87(2) and 0.44(5) for Mn and V respectively. These are confined in the bc plane with refined components m_{Mn} = (0, 3.27(2), 3.85(1)) μ_B and m_V = (0, 0.18(1), −0.17(1)) μ_B. Refinement of the magnetic structure considering only Mn moments was attempted, but resulted in fits of much lower quality (R_{mag} = 8.32%, χ^2 = 3.04), thus proving the necessity to include the vanadium contribution into the model. The slightly reduced moment values obtained for both sublattices reflect the discussed frustration in the system, previously observed from susceptibility data. Moreover, Mn and V spin sublattices are almost perpendicular, with a relative angle of 87.7(3)° between them. The WFM component observed in the M vs. H loops cannot be originated from antisymmetric Dzyaloshinskii-Moriya exchange interaction, since Mn (or V) atoms are centrosymmetric by neighboring pairs. Thus, one needs to consider the mΓ1$^+$ irreducible representation which would result in a ferromagnetic component along the x direction. This may also imply a lower symmetry. However, due to its small value of 0.07 μ_B no attempts of refinement were pursued.

The temperature variation of the Mn and V moments along with the fit to critical laws $\mu(T) = \mu(0)[1-(T/T_M)^\alpha]^\beta$ are shown in Fig. 3c. They result in T_M = 84.8(4) K and 31(2) K for Mn and V respectively, and α = 1.68(24) and β = 0.35(3) shared. The critical exponent β is close to the theoretical value of β = 0.34 for a

m_{Mn} = (0, 3.27(2), 3.85(1)) = 3.87(2) μ_B

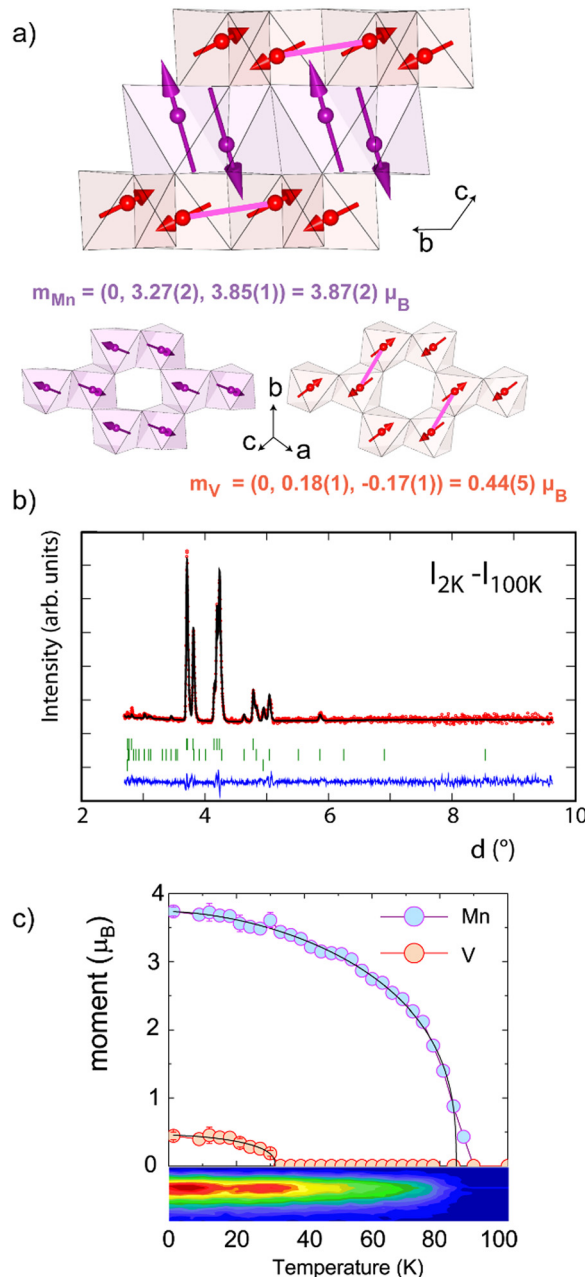m_V = (0, 0.18(1), −0.17(1)) = 0.44(5) μ_B

Fig. 3 (a) Spin order in the honeycomb layers with Mn and V moment components at 2 K, vanadium moments are scaled three times. (b) Difference between 2 K and 100 K neutron powder diffraction data with the refined k_0 = [0 0 0] magnetic model for MnVO$_3$-I. Small secondary magnetic signals from Mn$_3$V$_2$O$_8$ and MnO where considered as second and third phases respectively. (c) Temperature variation of the ordered Mn and V moments from neutron diffraction showing the critical law fit described in the text. The color intensity at the bottom shows the thermal evolution of the (−1 0 1) + k_0 magnetic reflection.

three-dimensional XY magnet, appropriate to $S = 5/2$ Mn^{2+} and $S = \frac{1}{2}$ V^{4+} spins laying in the bc plane but connected along z by Mn–V super-exchanges. Independent transitions for Mn and V are in good agreement with low temperature features in our bulk magnetic susceptibility measurements.[5]

The appearance of localized spins in the vanadium site of $MnVO_3$-I is somehow unexpected when compared with the other well studied triclinic distorted ilmenite-type vanadates AVO_3 (A = Mg and Co). $MgVO_3$, with a V–V dimer distance of ~ 2.78 Å, shows a non-magnetic nature due to the $3d_{xy}$ orbital pairing below 500 K.[10] $CoVO_3$, with a ~ 2.74 Å V–V distance, presents dimerized vanadium and is considered to be magnetic solely due to cobalt cations with a S = 3/2 state.[11] $MnVO_3$-I has a ~ 2.85 Å V–V dimer bond, also below the critical distance for direct exchange ($R_c \sim 2.94$ Å).[30,31] Along with the metal-like – semiconductor transition observed at 450 K, it is thus expected, by analogy, to be magnetic exclusively due to the manganese cations. However, due to ionic radii size of the Mn these bonds are longer than for $MgVO_3$ and $CoVO_3$, as well as the stronger magnetic interactions between d^5–d^1 Mn^{2+}–V^{4+} spins, results in low temperature localization of the V magnetic moments and the idea of a partial V–V dimerized state emerges. A resembling scenario appears in the GaV_4O_8, where besides the charge ordering behavior, a trimerized state is observed along with reduced spin localization at low temperature in the so-called "hybrid electrons".[33]

From extended Hückel tight-binding calculations (EHTB) in distorted V_6O_{24} honeycomb ring clusters isolated from AVO_3 (A = Mg, Co and Mn) we can clearly observe a bonding molecular orbital formation for the Mg and Co compounds. However, this is not visible for $MnVO_3$-I and it thus supports the conclusion that although there is a shortening in one of the V–V bonds, it is not sufficient to prevent the vanadium to magnetically order at low temperature. This implies that the $R_c \sim 2.94$ Å critical value for direct metal-metal bonding should be used as reference only. It also rises the question of whether the simple image of a Peierls-like transition is occurring in $MnVO_3$-I, where the metallic-like state should be ruled by the vanadium cations without intervention of the manganese, like in the $MnVO_3$-II perovskite analogue.[6] However, the observation of a first order structural transition at high-temperature and spin ordering in both Mn and V cations points toward an electronic correlation scenario. Besides these, the difference of 25 K between the metal-like – semiconductor and the structural transitions may indicate all together that a combination of both effects is taking part.

The transition is in fair agreement with the calculated density of states (DOS) for the high- (trigonal) and low-temperature (triclinic) $MnVO_3$-I using our experimental models in the AFM ($k_0 = [0\ 0\ 0]$ state), see Fig. 4b. The high spin local Mn^{2+} is well observed by half-occupied t_{2g} and e_g 3d bands split by ~ 1 eV. They show large exchange splitting between the majority and minority spins (~ 3 eV) for both structures. The calculated moment of ~ 4 μ_B for Mn (U = 1 eV) suggest a partial delocalization and Mn–O valence effects of the Mn d electrons. Moreover, the majority V^{4+} 3d bands (t_{2g} orbitals) mainly participate to the upper valence and lower conduction bands, with weak Mn–O–V hybridization. In the low temperature structure, a narrow gap of 0.2 eV opens in the t_{2g} manifold, in agreement with the semiconducting behavior observed. The V–V pairing accounts for the reduced localized moment on V
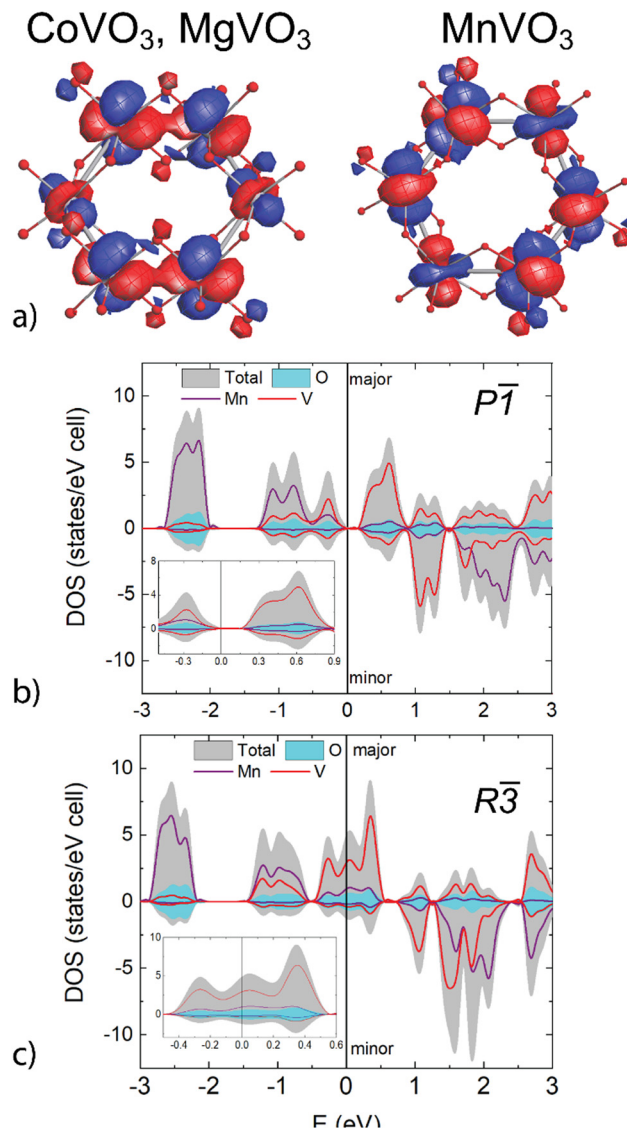

Fig. 4 (a) Extended Hückel tight-binding calculations of isolated V_6O_{24} units from $P\bar{1}$ $MgVO_3$ (identical to $CoVO_3$) and $MnVO_3$ where the dimerization is clear for the former. (b) and (c) Total and atomic projected DOS for $MnVO_3$-I in the low- and high-temperature polymorphs respectively (DFT, U = 1 eV, AFM spin configuration).

site (~ 0.66 μ_B/V). At high-temperature in the rhombohedral structure, the vanadium t_{2g} manifold degenerates and crosses the Fermi level within a metal-like state. However, an important localized moment of ~ 1 μ_B/V is calculated, which picture the main contribution of V atoms compared to O and Mn atoms in the narrow band crossing at the Fermi level. The different electronic behaviour of the triclinic and the trigonal phases show important coulombic effects, thus supporting the mixed scenario between electronic correlation and band effects discussed above, somehow similar to VO_2. Further studies of the accurate electronic structure should clarify what is the exact mechanism of the transition in $MnVO_3$-I. Moreover, the recognition of new systems similar to VO_2 is of current interest through the realization of thin film devices that may stabilize the high-pressure phase of $MnVO_3$-I.[34,35]

9242 | J. Mater. Chem. C, 2023, **11**, 9238–9244

This journal is © The Royal Society of Chemistry 2023

Conclusions

A metal-like – semiconductor transition was observed in the $MnVO_3$-I high pressure phase at 450 K. This is accompanied by a $R\bar{3}$ to $P\bar{1}$ structural transition where a Peierls-like V–V bond shortening occurs resembling that of VO_2. $MnVO_3$-I orders antiferromagnetically at $T_N = 77(1)$ K with a small ferromagnetic component of 0.07 μ_B at 2 K. NPD reveals a $k_0 = [0\ 0\ 0]$ magnetic propagation vector. The magnetic structure exhibits Mn and V spin components of 3.87(2) and 0.44(5) μ_B respectively. Contrary to the $MgVO_3$ and $CoVO_3$ analogues, EHTB calculations highlight that the dimerization is not full in $MnVO_3$-I and point towards a more complex electronic behaviour that may be clarified by RIXS experiments and more detailed calculations.

Author contributions

The study was designed by AMAL. Synthesis was performed by ESM and AMAL. Bulk magnetism and electric conductivity data were measured and analysed by ESM and AMAL. XPS experiments and analysis were performed by EPAL. Synchrotron diffraction data were collected and analysed by AM, FF, ESM and AMAL. Neutron diffraction data were collected and analysed by DK, ESM and AMAL. EHTB and DFT calculations were done by OM and AMAL. The paper was written with contributions from all authors.

Conflicts of interest

There are no conflicts to declare.

Acknowledgements

Notes and references

1 V. M. Goldschmidt, *Mat-Nature KI*, 1926, **2**, 117.
2 G. Demazeau, H. Huppertz, J. A. Alonso, R. Pottgen, E. Moran and J. P. Attfield, *Z. Naturforsch.*, 2006, **61b**, 1457.
3 A. Belik and W. Yi, *J. Phys.: Condens. Matter*, 2014, **26**, 163201.
4 E. Solana-Madruga and A. M. Arévalo-López, *J. Solid State Chem.*, 2022, **315**, 123470.
5 Y. Syono, S. Akimoto and Y. Endoh, *J. Phys. Chem. Solids*, 1971, **32**, 243.
6 M. Markkula, A. M. Arévalo-López, A. Kusmartseva, J. A. Rodgers, C. Ritter, H. Wu and J. P. Attfield, *Phys. Rev. B: Condens. Matter Mater. Phys.*, 2011, **84**, 094450.
7 B. L. Chamberland, *J. Solid State Chem.*, 1970, **1**, 138.
8 B. L. Chamberland, P. S. Danielson and C. W. Moeller, *J. Solid State Chem.*, 1978, **26**, 377.
9 B. L. Chamberland, *J. Solid State Chem.*, 1970, **2**, 521.
10 H. Yamamoto, S. Kamiyama, I. Yamada and H. Kimura, *J. Am. Chem. Soc.*, 2022, **144**, 1082.
11 S. Kamiyama, I. Yamada, M. Fukuda, Y. Okazaki, T. Nakamura, T. Nishikubo, M. Azuma, H. Kimura and H. Yamamoto, *Inorg. Chem.*, 2022, **61**, 7841.
12 J. R. Rea, P. W. Bless and E. Kostiner, *J. Solid State Chem.*, 1972, **5**, 446.
13 J. R. Rea and E. Kostiner, *J. Solid State Chem.*, 1973, **7**, 163.
14 S. Kamiyama, T. Sakakura, H. Kimura, H. Sagayama, S. Kishimoto, I. Yamada and H. Yamamoto, *Cryst. Growth Des.*, 2023, **23**, 2295.
15 S. Biermann, A. Poteryaev, A. I. Lichtenstein and A. Georges, *Phys. Rev. Lett.*, 2005, **94**, 026404.
16 M. W. Haverkort, Z. Hu, A. Tanaka, W. Reichelt, S. V. Streltsov, M. A. Korotin, V. I. Anisimov, H. H. Hsieh, H. J. Lin, C. T. Chen, D. I. Khomskii and L. H. Tjeng, *Phys. Rev. Lett.*, 2005, **95**, 196404.
17 D. Shiga, B. E. Yang, N. Hasegawa, T. Kanda, R. Tokunaga, K. Yoshimatsu, R. Yukawa, M. Ktamura, K. Horiba and H. Kumigashira, *Phys. Rev. B.*, 2020, **102**, 115114.
18 J. M. Tomczak, F. Aryasetiawan and S. Biermann, *Phys. Rev. B: Condens. Matter Mater. Phys.*, 2008, **78**, 115103.
19 R. Zhang, Q. S. Fu, C. Y. Yin, C. L. Li, X. H. Chen, G. Y. Qian, C. L. Lu, S. L. Yuan, X. J. Zhao and H. Z. Tao, *Sci. Rep.*, 2018, **8**, 17093.
20 F. Fauth, I. Peral, C. Popescu and M. Knapp, *Powder Diffr.*, 2013, **28**, S360.
21 F. Fauth, R. Boer, F. Gil-Ortiz, C. Popescu, O. Vallcorba, I. Peral, D. Fulla, J. Benach and J. Juanhuix, *Eur. Phys. J. Plus*, 2015, **130**, 160.
22 L. C. Chapon, P. Manuel, P. G. Radaelli, C. Benson, L. Perrott, S. Ansell, N. J. Rhodes, D. Raspino, D. Duxbury, E. Spill and J. Norris, *Neutron News*, 2011, **22**, 22.
23 J. Rodriguez-Carvajal, *Physica B*, 1993, **192**, 55.
24 V. Petricek, M. Dusek and L. Palatinus, *Z. Kristallogr.*, 2014, **229**, 345.
25 D. Dai, J. Ren, W. Lian and H. Whangbo, SAMOA (Structure and Molecular Orbital Analyzer), **http://primec.com/products/samoa/samoa.htm**.
26 G. Kresse and J. Hafner, *Phys. Rev. B: Condens. Matter Mater. Phys.*, 1993, **47**, 558.
27 J. B. Goodenough, G. Dutta and A. Manthiram, *Phys. Rev. B: Condens. Matter Mater. Phys.*, 1991, **43**, 10170.
28 J. B. Goodenough, *Magnetism and the chemical bond*. Wiley Interscience, New York, 1963.
29 I. D. Brown and D. Altermatt, *Acta Crystallogr., Sect. B: Struct. Sci.*, 1985, **41**, 244.
30 E. Morosan, J. Fleitman, T. Klimczuk and R. J. Cava, *Phys. Rev. B: Condens. Matter Mater. Phys.*, 2007, **76**, 144403.
31 H. T. Stokes, D. M. Hatch and B. J. Campbell, *ISODISTORT, ISOTROPY Software Suite*, **iso.byu.edu**.
32 B. J. Campbell, H. T. Stokes, D. E. Tanner and D. M. Hatch, *J. Appl. Cryst.*, 2006, **39**, 607.

33 C. Aguilar-Maldonado, O. Mentré, A. A. Tsirlin, C. Ritter, A. Missiul, F. Fauth and A. M. Arévalo-López, *Mater. Horiz.*, 2021, **8**, 2325.

34 J.-P. Pouget, *C. R. Phys.*, 2021, **22**, 37.

35 J. del Valle, N. M. Vargas, R. Rocco, P. Salev, Y. Kalcheim, P. N. Lapa, C. Adda, M.-H. Lee, P. Y. Wang, L. Fratino, M. J. Rozenberg and I. K. Schuller, *Science*, 2021, **373**(6557), 907.

9244 | *J. Mater. Chem. C*, 2023, **11**, 9238–9244

This journal is © The Royal Society of Chemistry 2023